

Predicting Glass-to-Glass and Liquid-to-Liquid Phase Transitions in Water

Robert F. Tournier^{1,2}

¹Univ. Grenoble Alpes, Inst. NEEL, F-38042 Grenoble Cedex 9, France

²CNRS, Inst. NEEL, F-38042 Grenoble, France

E-mail address: robert.tournier@neel.cnrs.fr

Abstract:

Glass-to-glass and liquid-to-liquid phase transitions are observed in bulk and confined supercooled water, with or without applied pressure. They result from the competition of two liquid phases separated by an enthalpy difference depending on temperature. The classical nucleation equation of these phases is completed by this quantity existing at all temperatures, a pressure contribution, and an enthalpy excess. Thermodynamic properties, double glass transition temperatures, sharp enthalpy and volume changes are predicted in agreement with experimental results. The first-order transition line between fragile and strong liquids joins three critical points. The glass phase above T_g becomes a third liquid phase.

Introduction: Multiple liquid-to-liquid phase transitions (LLPTs) observed in several metallic glass-forming melts have already been predicted using a classical nucleation equation completed by an enthalpy difference of two liquid phases depending on the square of the reduced temperature $\theta = (T - T_m)/T_m$, T_m as the melting temperature [1]. The objectives of this paper are to extend the application of this renewed equation to the thermodynamic properties of water, to explain the occurrence of glass-to-glass phase transitions in amorphous water, and to show that the high-density phases obtained under pressure are ultrastable glass phases analogous to those produced by vapor deposition at temperatures close to T_g [2-5].

First-order transformations under pressure induce high density amorphous phase [6-12], because the pressure decreases the enthalpy and facilitates the glass transformation towards an equilibrium phase of higher density. These enthalpy and entropy changes cannot exceed the value of the frozen enthalpy and entropy [13]. Any glass freezes enthalpy and entropy below T_g , which are available for exothermic relaxation or first-order transitions.

The water glass state is obtained by vapor deposition, liquid hyperquenching, confined water cooling, and high pressure applied to ice [14]. A warm-up of bulk amorphous water produces an endothermic event just below the crystallization temperature, occurring at around 136 K [15-17]. The glass transition is characterized by a specific heat jump preceding the occurrence of crystallization [17]. Applying high pressure to ice reduces T_m and produces liquid and amorphous water. Sharp transformations viewed as first-order transitions are observed under pressure at 77 K, and at higher temperatures. These findings show that a bulk amorphous liquid having low density can be transformed under pressure into high-density amorphous liquid [8,11,17]. Three glass states have been identified under pressure: low density amorphous liquid (LDA); high density amorphous liquid (HDA); and very high density amorphous liquid (VHDA). Transformations of LDA to HDA and VHDA are observed after increasing pressure up to 16 kbar, and decompression down to residual pressures p at temperatures smaller than T_g . Some VHDA,

HDA and LDA are studied after complete decompression down to 77 K [2,12]. HDA obtained after decompression at 77 K down to 100 bar is also transformed by heating at ~140K in LDA [10]. The HDA phase is recovered by a new compression at $p=0.32\text{GPa}$.

Measurements of water confined within silica gel in 1.1nm pores show the existence of a broad and high specific heat peak at 227.5K (-45.6°C), and two heat flow changes at 130–143 and 160–190 K, showing the presence of two glass transitions [19,20]. A pronounced minimum of compressibility is still observed in water at a temperature of +45.5°C, which is symmetrical with regard to T_m at ambient pressure of the transition at -45.6°C [21,22]. A specific heat increase below 273 K is still observed in bulk supercooled water at ambient pressure down to the crystallization temperature [14,23], confirming the existence, in the absence of crystallization, of a liquid-to-liquid phase transition (LLTP) at 227.5K [20,24].

These phenomena are attributed, in the first model of two liquids, to the existence of a critical point leading to a line of first-order LLPTs [22,25-28]. The two liquids have the same chemical composition and contain low- and high-density species forming differently bonded domains. Such LLPTs form part of the general phenomenology for a wide range of liquids [29]. These ideas are successful to explain the existence of LLPTs, but are not able to predict glass thermodynamic properties, because they view them as a result of freezing, instead of a thermodynamic transition related to the difference of enthalpy of Phase 1 and Phase 2. The LLPT at 227.5 K looks like a first-order transformation of strong glass to fragile liquid [26].

In this paper, the glass transition is viewed as having a thermodynamic origin. There are many models describing it as a true phase transformation and experimental evidences in favor of this interpretation. The glass transition is seen as a manifestation of critical slowing down near a second-order phase transition with the possible existence of several classes of universality [30]. A model predicting the specific heat jump is based on a percolation-type phase transition with formation of dynamical fractal structures near the percolation threshold [31-37]. Macroscopic percolating clusters formed at the glass transition have been visualized [37]. High precision measurements of third- and fifth-order non linear dielectric susceptibilities lead to a fractal dimension $d_F=3$ for the growing transient domains [38]. An observation of structural characteristics of medium-range order with neutrons and X-rays leads to $d_F=2.31$ [39]. An other model entirely based on thermodynamics predict the specific heat jump of strong and fragile glasses and liquid-to-liquid phase transitions [1,40]. For that, the classical nucleation equation is completed by introducing the enthalpy savings $-\epsilon_{ls}\times\Delta H_m$, $-\epsilon_{gs}\times\Delta H_m$, and $-\Delta\epsilon_{lg}\times\Delta H_m$, respectively, associated with the growth critical nucleus formation leading to Phase 1 and Phase 2 above T_g and Phase 3 below T_g , where ΔH_m is the melting heat [40]. The enthalpy difference $\Delta\epsilon_{lg}\times\Delta H_m$, associated with the formation of vitreous Phase 3 below T_g , is then equal to $(\epsilon_{ls}-\epsilon_{gs})\times\Delta H_m$. The coefficients ϵ_{ls} and ϵ_{gs} are linear functions of $\theta^2=(T-T_m)^2/T_m^2$, as shown by studying supercooling rate maxima of liquid elements [39]. A positive sign of $\Delta\epsilon_{lg}=(\epsilon_{ls}-\epsilon_{gs})$ above T_g and T_m at a reduced temperature θ shows that Phase 1 is favored; a negative value reveals that it is Phase 2 [1]. The first-order transition to a glass of confined liquid helium under pressure has been described using $\epsilon_{ls0}=\epsilon_{gs0}=0.217$ [42]. This glass is ultrastable because there is no more enthalpy to relax in this state. These values of ϵ_{ls0} and ϵ_{gs0} , determined in many pure liquid elements at their melting temperature T_m , correspond to the Lindemann coefficient 0.103 [43]. The transformation temperature T_{sg} of glasses in ultrastable phases with higher density has been defined as a function of a frozen enthalpy excess $\Delta\epsilon\times\Delta H_m$. The denser ultrastable glass attains its lowest enthalpy at a transformation temperature T_{sg}

for $\Delta\varepsilon = (\varepsilon_{ls0} - \varepsilon_{gs0})$ [5]. The transformation of Phase 3 into polyamorphous ultrastable phases under pressure produces sharp enthalpy changes that are predicted by this model.

2-Basic equations applied to water

The completed nucleation equation is given by (1):

$$\Delta G = \frac{4\pi R^3}{3} \Delta H_m / V_m \times (\theta - \varepsilon) + 4\pi R^2 (1 + \varepsilon) \sigma_1 \quad (1)$$

where ΔG is the Gibbs free energy change per volume unit, associated with the formation of a spherical growth nucleus of radius R , ε is a fraction of the melting enthalpy ΔH_m equal to ε_{ls} for a nucleus of Phase 1, ε_{gs} for a nucleus of Phase 2, $\Delta\varepsilon_{lg}$ for a nucleus of Phase 3, V_m the molar volume, and $\theta = (T - T_m) / T_m$ the reduced temperature. The melting heat ΔH_m and T_m are assumed to be the same whatever the nucleus radius R is, and not dependent on R . The critical nucleus can give rise to Phase 1 or Phase 2, or amorphous Phase 3, or various LLPT, according to the thermal variations of ε . The new surface energy is $(1 + \varepsilon) \times \sigma_1$ instead of σ_1 . The classical equation is obtained for $\varepsilon = 0$ [44]. The homogeneous nucleation temperatures are $\theta_{n-} = (\varepsilon - 2) / 3$ for $\theta < 0$ and $\theta_{n+} = \varepsilon$ for $\theta > 0$ [1,40]. The critical radius is infinite at the homogeneous nucleation temperature obtained for $\theta = \varepsilon$ instead of $\theta = 0$ for the classical equation. A catastrophe of nucleation occurs at $\theta = \varepsilon$ for crystals protected against surface melting [45].

The coefficients ε_{ls} and ε_{gs} in (2) and (3) are values of $\varepsilon(\theta)$, respectively, leading to a nucleus formation having the critical radius for Phase 1 and Phase 2 formations under pressure:

$$\varepsilon_{ls}(\theta) = \varepsilon_{ls0} (1 - \theta^2 \times \theta_{0m}^{-2}) + P_1, \quad (2)$$

$$\varepsilon_{gs}(\theta) = \varepsilon_{gs0} (1 - \theta^2 \times \theta_{0g}^{-2}) - \Delta\varepsilon + P_2, \quad (3)$$

where $\Delta\varepsilon$ is the coefficient of enthalpy excess in Phase 2 being frozen after quenching Phase 1; $P_1 = (p - p_0) \times V_{m1} / \Delta H_m$ and $P_2 = (p - p_0) \times V_{m2} / \Delta H_m$ are the contributions of the pressure p to the enthalpy coefficients ε_{ls} and ε_{gs} , and p_0 is the ambient pressure [5]. The coefficients ε_{ls} and ε_{gs} are equal to zero at the reduced temperatures θ_{0m} and θ_{0g} for $\Delta\varepsilon = 0$ and $P_1 = 0$, and correspond to the Vogel-Fulcher-Tammann temperatures above and below T_g , respectively. Equations (2) and (3) are respected at the homogeneous nucleation temperatures θ_{n-} in Phase 1 and Phase 2. Equation (4) determines θ_{n-} of Phase 2 combining (3) with $\theta_{n-} = (\varepsilon_{gs} - 2) / 3$ [40]:

$$\theta_{n-}^2 \times \varepsilon_{gs0} \times \theta_{0g}^{-2} + 3\theta_{n-} + 2 - \varepsilon_{gs0} + \Delta\varepsilon - P_2 = 0 \quad (4)$$

The solutions for θ_{n-} are given by (5):

$$\theta_{n-} = (-3 \pm [9 - 4(2 - \varepsilon_{gs0} + \Delta\varepsilon - P_2) \varepsilon_{gs0} / \theta_{0g}^2]^{1/2}) \theta_{0g}^2 / (2\varepsilon_{gs0}) \quad (5)$$

θ_{n-} of Phase 2 for the sign + is called θ_2 , given by (5).

Equation (6) determines the homogeneous nucleation temperature θ_{n-} of Phase 1 combining (2) at this temperature with $\theta_{n-}=(\varepsilon_{ls}-2)/3$:

$$\theta_{n-}^2 \times \varepsilon_{ls0} \times \theta_{0m}^{-2} + 3\theta_{n-} + 2 - \varepsilon_{ls0} - P_1 = 0 \quad (6)$$

The reduced homogeneous nucleation temperature θ_{n-} of Phase 1 under pressure in (7) is deduced from (6):

$$\theta_{n-} = (-3 \pm [9 - 4(2 - \varepsilon_{ls0} - P_1)\varepsilon_{ls0} / \theta_{0m}^2]^{1/2})\theta_{0m}^2 / (2\varepsilon_{ls0}) \quad (7)$$

θ_{n-} in (7) is called θ_1 for the sign +. The glass transition occurs at θ_g when $\varepsilon_{ls}(\theta)$ in (2) is equal to $\varepsilon_{gs}(\theta)$ in (3). θ_1 and θ_2 are equal to θ_g in strong glasses because $\varepsilon_{ls}(\theta_g)=\varepsilon_{gs}(\theta_g)$ for $\Delta\varepsilon=0$ and $P_1=P_2=0$.

As water is a strong glass at low temperatures, the coefficients ε_{gs0} in (8) and ε_{ls0} in (9), deduced from (4) with $P_2=0$ and from (6) with $P_1=0$ and $\Delta\varepsilon=0$, are determined from the knowledge of θ_g , θ_{0g} , and θ_{0m} [40]:

$$\varepsilon_{gs0} = \frac{3\theta_g + 2}{1 - \theta_g^2 / \theta_{0g}^2} \quad (8)$$

$$\varepsilon_{ls0} = \frac{3\theta_g + 2}{1 - \theta_g^2 / \theta_{0m}^2} \quad (9)$$

where the reduced temperatures θ_{0g} and θ_{0m} are equal to -1 and -2/3, respectively, because the Vogel-Fulcher Tamman temperatures are equal to 0 K below T_g and to $T_m/3$ above T_g for many pure strong liquid elements [41]. With $T_g=136.6$ K, $\theta_g=-0.5$, ε_{gs0} is equal to 0.66667 and ε_{ls0} to 1.14286. The frozen enthalpy at T_g is equal to the minimum value $-0.37037 \times \Delta H_m$ of $(\varepsilon_{ls}-\varepsilon_{gs}) \times \Delta H_m$ obtained for $\varepsilon_{ls}=0$ at $\theta=\theta_{0m}=-2/3$. The heat capacity jump at T_g is equal to: $(d\varepsilon_{ls}/dT - d\varepsilon_{gs}/dT) \times \Delta H_m = -1.905 \times \Delta H_m / T_m = 41.9 \text{ JK}^{-1} \text{ mole}^{-1}$ in agreement with old measurements [17], as shown in Figure 1.

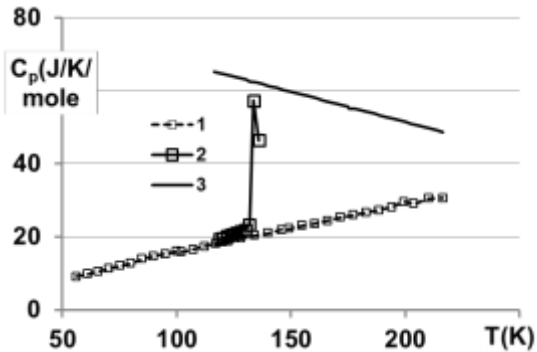


Figure 1: 1. Heat capacity of hexagonal ice [10]; 2. Heat capacity jump at 133.6 K [10]; 3. Supercooled water heat capacity calculated with the derivative $(d\varepsilon_{ls}/dT - d\varepsilon_{gs}/dT) \times \Delta H_m$.

For confined supercooled water in pores of radius $R=0.55$ nm [19,20], θ_2 is equal to -0.16715 (227.5K) for $P_2=0.8505$ and $\Delta\varepsilon=0$ in (5). Using the Young-Laplace equation, Δp is equal to $2\gamma/R=0.31\pm 0.02$ GPa, with a value of the surface tension $\gamma=0.085\pm 0.005$ J/m² at 227.5K extrapolated from its thermal variation above 250K [23]. The enthalpy coefficient P_2 is deduced to be close to 0.8505 with $V_{m2} \cong 16.5 \times 10^{-6}$ m³ and $p=0.31$ GPa.

The enthalpy difference coefficient $\Delta\varepsilon_{lg}$ associated with vitreous and liquid Phase 3 is given by (10) under pressure p :

$$\Delta\varepsilon_{lg}(\theta) = (\varepsilon_{ls} - \varepsilon_{gs}) = \varepsilon_{ls0} - \varepsilon_{gs0} + \Delta\varepsilon + P_1 - P_2 - \theta^2 \left(\frac{\varepsilon_{ls0}}{\theta_{0m}^2} - \frac{\varepsilon_{gs0}}{\theta_{0g}^2} \right) \quad (10)$$

The difference $\Delta P=(P_1-P_2)=\delta V \times p/\Delta H_m$ is proportional to the volume change δV , and to the pressure p at the transformation temperature θ . ΔP is equal to zero for $\delta V=0$ in the absence of latent heat. The homogeneous nucleation temperature of Phase 3 also occurs for $\Delta\varepsilon_{lg}=0$ with $\Delta\varepsilon=0$ because Phase 1 and Phase 2 have the same homogeneous nucleation temperature $\theta_1=\theta_2=\theta_g$.

A sharp enthalpy difference between nonrelaxed Phase 3 and fully relaxed Phase 3 can be induced in all glasses below T_g for $\Delta\varepsilon_{lg}=0$ in (10), when an enthalpy excess coefficient $\Delta\varepsilon$ exists after rapid cooling, as already described for an ultrastable glass formation [5]. This enthalpy difference is equal to $2 \times \Delta\varepsilon_{lg}(\theta) \times \Delta H_m$ because this enthalpy difference cannot exceed the frozen enthalpy which is available at any temperature below T_g . This transformation temperature T_{sg} for a stable glass formation given in (11) is also induced by pressure. It depends on δV and on the value of $\Delta\varepsilon$ at this temperature.

$$\theta_{sg} = - \left[(\varepsilon_{ls0} - \varepsilon_{gs0} + \Delta\varepsilon + \Delta P) / (\varepsilon_{ls0} \theta_{0m}^{-2} - \varepsilon_{gs0} \theta_{0g}^{-2}) \right]^{1/2} \quad (11)$$

Such sharp transitions are observed after complete decompression of VHDA at 77K from various pressures, and are reproduced in Figure2 [46].

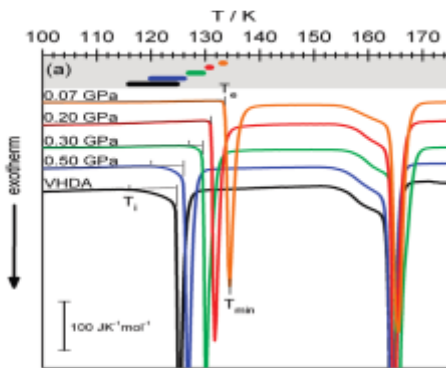


Figure 2: Reprinted from [46, Figure 3]. “DSC scans recorded at a rate of 10 K/min. The DSC output signal was normalized to 1 mol. The samples were heated from 93 to 253 K; thermograms are plotted in the temperature range of 100–175 K. Shown are VHDA (black line) and four samples made by decompression of VHDA at 140 K to 0.5 (blue line), 0.3 (green line), 0.2 (red line), and 0.07 GPa (orange line). First exothermic peak: transition to LDA; second exothermic peak: crystallization to cubic ice. The

bars in the top part indicate the difference between T_i and T_e , which is a measure of the relaxation state of the sample.” There is no detectable endothermal event at $T=136.6K$.

Several lines of $\Delta\epsilon_{lg}$ given by (10) are represented in Figure 3. The line $\Delta\epsilon_{lg}=0$ is plotted versus θ for $P_1-P_2=0$ and $\Delta\epsilon = -1.14286\times(1-2.25\times\theta^2)+0.66667\times(1-\theta^2)$ because $\Delta\epsilon_{lg}$ is negative when $\Delta\epsilon=0$. This enthalpy excess increases the density of the LDA phase below $\theta=\theta_{sg}$. The coefficient $\Delta\epsilon$ sharply disappears at $\theta=\theta_{sg}$, seen as a first “ T_g ” and decreases the density. Line 1 corresponds to nonrelaxed Phase 3, with $\Delta\epsilon_{lg}$ given by (10) for $\Delta\epsilon=0$ and $P_1-P_2=0$. Line 2 represents $\Delta\epsilon_{lg}$ of fully-relaxed Phase 3 above θ_{sg} . Using a linear approximation, this $\Delta\epsilon_{lg}$ is equal to about $2\times 0.37037\times(T_{sg}-T_g)/(T_g-91)=0.00407\times(T_{sg}-136.6)$. The available latent heats $\Delta\epsilon_{lg}\times\Delta H_m$ along Line 2 are in rough agreement with those observed in Figure 2.

The glass transition without applied pressure is equal to 136.6K. On Line 3 of Figure 3, the first T_g of confined water in 1.1nm pores is 115K, whereas the second T_g under Laplace pressure with $T_m=273.1K$ is 162K [19]. Several other examples of double transition are presented in Figure 3 and correspond to those of Figure 2.

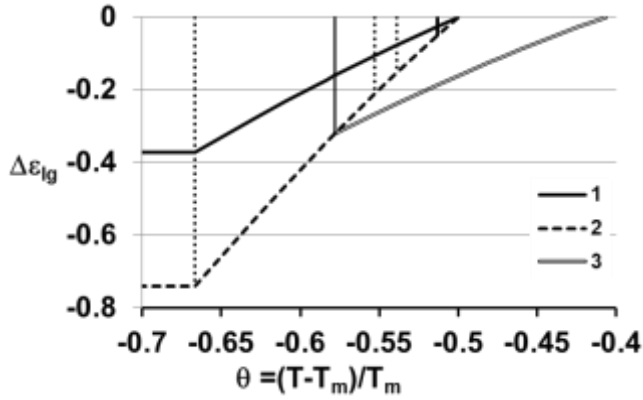


Figure 3: Reduced temperatures θ_{sg} along the line $\Delta\epsilon_{lg}=0$ and latent heat coefficients $\Delta\epsilon_{lg}$ associated with the glass-to-glass transformations after decompression. Curves numbered from 1 to 4: 1. $\Delta\epsilon_{lg}(\theta)$ given by (10) of nonrelaxed Phase 3 with $\Delta\epsilon=0$, $\Delta P=0$, $\theta_g=-0.5$ ($T_g=136.6K$); 2. Equilibrium enthalpy coefficient $2\times\Delta\epsilon_{lg}(\theta)$ of ultrastable Phase 3 crossing $\theta_g=-0.5$ ($T_g=136.6K$) without endothermal event; 3. $\Delta\epsilon_{lg}(\theta)$ starting after transition from $\theta_{sg}=-0.578$, $T_{sg}=115.3K$ with $\Delta\epsilon=0$ and $\Delta P=-0.1608$, corresponding to the Laplace pressure at 162K in 1.1nm pores [19] and finishing at $\theta_g=-0.4069$, $T_g=162K$. Other reduced temperatures θ_{sg} equal to -0.66667, -0.55277, -0.5387, and -0.51307, corresponding to $T_s=91$, 122.2, 126, and 133K, respectively.

The glass transition at 136.6K is not detected in Figure 2 above θ_{sg} . Then, the transitions at T_{sg} decreasing the density give rise to amorphous ice instead of fully relaxed Phase 3. The latent heat at its crystallization temperature at 164K would have to depend on the exothermic heat recovered at θ_{sg} . This absence of transition at 136.6K confirms recent findings that the sharp transitions of polyamorphous LDA phases at $p=0$ [46] lead to amorphous ice resulting from molecular reorientation processes [47]. The enthalpy coefficient along Line 2 in Figure 3 cannot be attained by Phase 3, because the weakest density of Phase 3 would be smaller than that of ice. The glass phase is recovered in relaxed samples because their density is higher along Line 1 [47].

There are two regions of crystallization of water around 230–250K and 135–165K. Supercooled water undergoes a first-order phase transition that separates fragile from strong states. Fragile liquids have values of ε_{ls0} given in (12) [40]:

$$\varepsilon_{ls}(\theta = 0) = \varepsilon_{ls0} + P_1 = 1.5 \times \theta_1 + 2 + P_1 = a \times \theta_g + 2 + P_1, \quad (12)$$

where $a=1$ leads to a specific heat excess $\Delta C_p(T)$ of the supercooled melt at the glass transition equal to $1.5 \times \Delta H_m / T_m$ [48-50]. The reduced temperature θ_{0m} is given by (13), and is a double solution for (6):

$$\theta_{0m}^2 = \frac{8}{9} \varepsilon_{ls0} - \frac{4}{9} \varepsilon_{ls0}^2. \quad (13)$$

New parameters ε_{gs0} and θ_{0g} are fixed at T_g and below T_g by (14) and (15) to have a double solution for (4) with $a=1$ because $a < 1$ leads to a too high nucleation temperature T_1 in Phase 1; ε_{gs0} is maximized by (14) and (15) [40]:

$$\varepsilon_{gs}(\theta = 0) = \varepsilon_{gs0} + P_2 = 1.5 \times \theta_g + 2 + P_2, \quad (14)$$

$$\theta_{0g}^2 = \frac{8}{9} \varepsilon_{gs0} - \frac{4}{9} \varepsilon_{gs0}^2. \quad (15)$$

The LLPT in fragile confined water occurs at 227.5K ($\theta_{LL} = -0.16715$) [19]. This temperature does not depend on pressure because it occurs when $\Delta \varepsilon_{lg}$ is equal to 0 in (10), with $\Delta \varepsilon = 0$, $P_1 = P_2$, and because $\Delta \varepsilon_{lg} = 0$ is still reproduced in (10) at the isothermal compressibility minimum temperature $\theta_{LL} = -0.16715$, $T_{LL} = 318.8K$, with P_1 and $P_2 = 0$, $\Delta \varepsilon = 0$ [22,51,52]. The value $a=1$ used in Figure 4 leads to $\varepsilon_{ls0} = 1.7953$, $\varepsilon_{gs0} = 1.69295$, $\theta_{0g}^2 = 0.23103$, $\theta_{0m}^2 = 0.16333$ with $\theta_g = -0.2047$ and to $T_1 = 235.9K$ in good agreement with a maximum supercooling of water equal to 35K. The coefficients ε_{ls} and ε_{gs} of fragile liquids are equal to 1.5 at $\theta = \theta_{LL}$ while those of strong liquids are respectively equal to 1.07102 and 0.42298. Under these conditions, the water specific heat increase up to 81 J/mole at $\theta_{LL} = -0.16715$ [19] is due to a LLPT [22,25-28]. This increase is not only observed at zero pressure, but also under a Laplace pressure of $0.31 \pm 0.02 GPa$ in 1.1 nm pores, slightly increasing with decreasing temperature [19,53-56]. In Figure 4, the LLPT at 227.5K and zero pressure is accompanied during heating by an exothermic latent heat of $(1.5 - 1.07102 - 0.42298) \Delta H_m = 0.006 \times \Delta H_m$ associated with Phase 1 and Phase 3 transformations because glass Phase 3 is transformed in liquid Phase 3 at T_g and continues to exist as a liquid phase above T_g . As expected [22-28], a critical point is close to $p=0$ in these conditions.

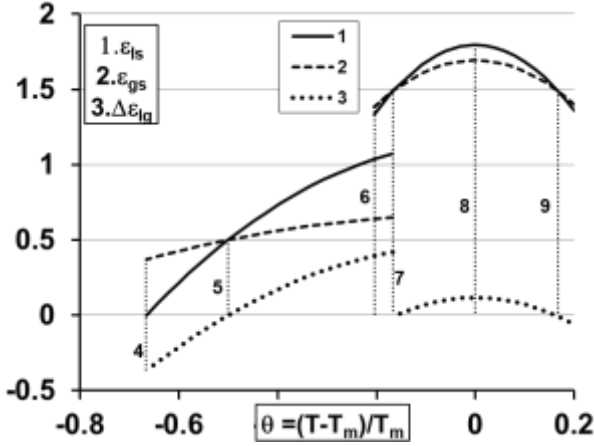


Figure 4: The enthalpy coefficients ε_{is} , ε_{gs} and $\Delta\varepsilon_{lg}$ of Phase 1, Phase 2 and Phase 3, $P=0$. For the strong liquids at $\theta_{LL}=-0.16715$, $\varepsilon_{is}=1.07102$, $\varepsilon_{gs}=0.64804$, $\Delta\varepsilon_{lg}=0.42298$ and at $\theta_g=-0.5$, $\varepsilon_{is}=\varepsilon_{gs}=0.5$. For the fragile liquids at $\theta_{LL}=-0.16715$, $\varepsilon_{is}=\varepsilon_{gs}=1.5$. Curves numbered from 1 to 3: 1- $\varepsilon_{is}(\theta)$ of Phase 1 given by (2) below $\theta_{LL}=-0.16715$ in the strong water and above in the fragile one; 2- $\varepsilon_{gs}(\theta)$ of Phase 2 given by (3) below and above $\theta_{LL}=-0.16715$; 3- $\Delta\varepsilon_{lg}(\theta)$ of Phase 3 below and above θ_{LL} . Temperatures numbered from 4 to 9: 4- The frozen enthalpy coefficient $\Delta\varepsilon_{lg}$ equal to -0.37037 at $\theta=-2/3$; 5- The glass transition $\theta_g=-0.5$ ($T_g=136.6$ K); 6- $\theta_g=-0.2047$ of the fragile water in the absence of LLTP; 7- At $\theta_{LL}=-0.16715$, $T_{LL}=227.5$ K, the LLTP for $\Delta\varepsilon_{lg}=0$; 8- $\theta=0$ the melting temperature at $T_m=273.14$ K; 9- For $\theta=0.16715$, $\Delta\varepsilon_{lg}=0$ at the isothermal compressibility minimum temperature 318.7 K.

2- Transformation of LDA to ultrastable HDA under pressure

High pressure applied to ice samples followed by complete decompression induces an LDA phase [11]. In all experiments involving high pressures, some enthalpy excess $\Delta\varepsilon$ due to the Phase 1 quenching is frozen because the melting temperature T_m is strongly decreased, and the sample is cooled during decompression from temperatures much higher than T_m . Compression experiments of this LDA phase at various temperatures transform it into an HDA phase at a well-defined pressure p , inducing a sharp transition. The volume change δV in (10) does not depend on the pressure p and is equal to 0.22×10^{-6} m³/g, as shown in Figure5 [9].

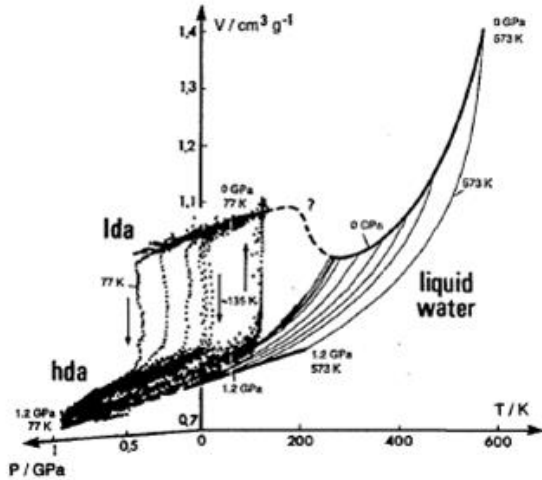


Figure 5: Specific volume versus pressure (GPa) and Temperature (K). “Low density amorphous to high density amorphous transformations under pressure occur for $p=0.55, 0.45, 0.38, 0.32, 0.05$ GPa and $T=77, 100, 121, 135, 135$ K respectively. Liquid water under 1.2 GPa and 0 pressures is also represented versus temperature. The linkage between LDA and liquid state at zero pressure occurs at 227K. The liquid at zero pressure corresponds to Phase 1” Reprinted from [9, Figure 4].

The equilibrium enthalpy change under pressure is equal to $\Delta P = p \times \delta V / \Delta H_m$. Fully relaxed Phase 3 (HDA) is expected to have a maximum enthalpy difference with nonrelaxed Phase 3 (LDA) equal to $-0.37037 \times \Delta H_m$, as shown by the difference between Line 1 and Line 2 at $\theta = -2/3$ in Figure 4. In Figure 6, $\Delta \varepsilon_{lg}$ values are represented as a function of θ and calculated from (11). The values of $\Delta \varepsilon$ and ΔP at the temperature of sharp transitions given in the Figure 5 caption are indicated in the Figure 6 caption. The values of T_m under pressure are those of hexagonal ice [8]. Those of $\Delta \varepsilon$ decrease with temperature and disappear at $\theta = \theta_{sg}$, as already observed in ethylbenzene [5,56]. A rapid quenching is freezing Phase 1 instead of Phase 2 and an enthalpy excess $\Delta \varepsilon$ is added to Phase 2 as shown in Figure 6 below $\theta = \theta_{sg}$. This enthalpy excess has been observed in several strong or fragile glasses below T_g [57,58]. The values of ΔP are proportional to the pressure p . The maximum value $\Delta \varepsilon_{lg} = -0.37037$ is obtained for all pressures $p \leq 0.55$ GPa. Then, the HDA phase corresponds to the largest enthalpy change associated with the formation of an ultrastable glass phase. The calculated volume change $0.224 \times 10^{-6} \text{ m}^3/\text{g}$ is constant under various pressures p , and equal to the experimental value. The highest density of the HDA phase is obtained at 77K. The polyamorphous ultrastable glass phase becomes less dense at higher temperatures T_{sg} given by (11). The LDA-to-HDA transformation occurring for $p=0.32$ GPa in the interval 130–140K is reversible when the pressure is decreased down to $p=0.05$ GPa. The glass transition falls from 150.6K to 139.6K when p is reduced, whereas the LDA phase is recovered. This reversibility proves the first-order character of the transition [9]. The enthalpy excess $\Delta \varepsilon \times \Delta H_m$ of LDA is fully recovered at $T = T_{sg}$ and $p=0$ because the pressure decreases the enthalpy and the volume by a constant quantity while the enthalpy relaxation increases the glass volume towards that of ice. It is only relaxed at $p=0$ increasing the volume and leading to amorphous ice, as shown in Figure 2.

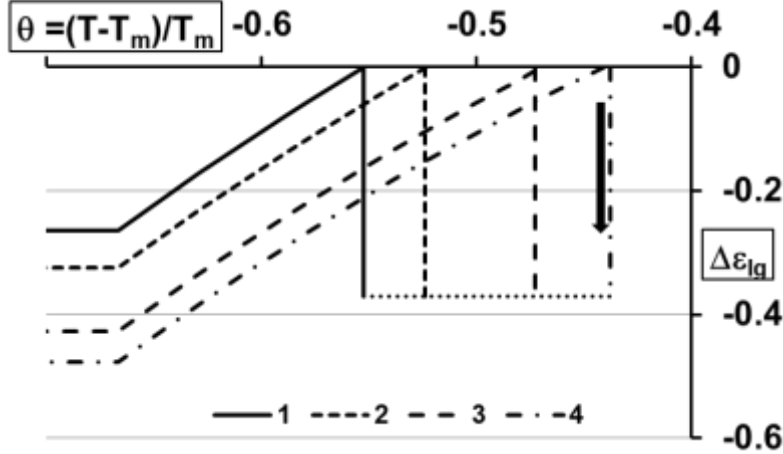


Figure 6: Calculated reduced temperatures θ_g of low density amorphous (LDA)-to-high density amorphous (HDA) transformations under constant pressure p using (11) in agreement with experiments shown in Figure 5. The temperatures θ_{sg} are obtained for $\Delta\epsilon_{lg}=0$. Curves numbered from 1 to 5: 1. $\Delta\epsilon_{lg}(\theta)$ for $\Delta\epsilon=\epsilon_{ls0}-\epsilon_{gs0}=0.47619$, $\Delta P=-0.37037$, $p=0.55\text{GPa}$, $T_m=172\text{K}$, $\theta_{sg}=-0.55278$, $T_{sg}=77\text{K}$; 2. $\Delta\epsilon_{lg}(\theta)$ for $\Delta\epsilon=0.349$, $\Delta P=-0.30103$, $p=0.45\text{GPa}$, $T_m=210\text{K}$, $\theta_{sg}=-0.52357$, $T_{sg}=100\text{K}$; 3. $\Delta\epsilon_{lg}(\theta)$ for $\Delta\epsilon=0.199$, $\Delta P=-0.25589$, $p=0.38\text{GPa}$, $T_m=228\text{K}$, $\theta_{sg}=-0.46918$, $T_{sg}=121\text{K}$; 4. $\Delta\epsilon_{lg}(\theta)$ for $\Delta\epsilon=0.104$, $\Delta P=-0.21549$, $p=0.32\text{GPa}$, $T_m=240\text{K}$, $\theta_{sg}=-0.43757$, $T_{sg}=135\text{K}$; 5. At $T=T_{sg}$, the glass enthalpy coefficient is lowered by -0.37037 corresponding to the formation of a polyamorphous phase after a constant volume change $\delta V=-0.224\times 10^{-6}\text{m}^3/\text{g}$.

The ultrastable phase is stabilized under pressure at temperatures smaller than T_{sg} , and disappears far beyond T_{sg} , as shown in Figure 7. The glass transition temperatures of ultrastable phases are occurring for $\Delta\epsilon_{lg}=0$ in (10) assuming that $\Delta\epsilon=0$ and ΔP is equal to the values given in the Figure 6 caption. They are represented in Figure 7, and are varying from 131.5K for $p=0.55\text{GPa}$ to 150.5K for $p=0.32\text{GPa}$. The pressure contribution $\Delta P\times\Delta H_m$ disappears at this new T_g . These glass transitions are masked by crystallization.

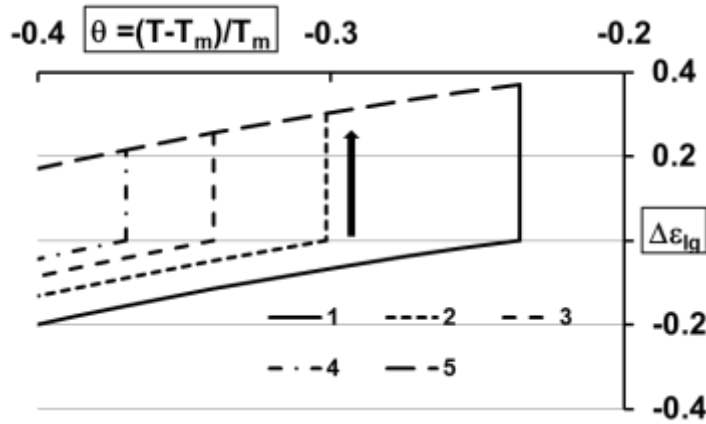


Figure 7: Calculated glass transition temperatures T_g of supercooled water under pressure p . The glass transitions occur for $\Delta\epsilon_{lg}=0$. The lines $\Delta\epsilon_{lg}(\theta)$ numbered 1–4 complete those of Figure 6 at higher

temperatures with $\Delta\varepsilon=0$: 1. $\Delta P=0.37037$, $p=0.55\text{GPa}$, $T_m=172\text{K}$, $\theta_g=-0.2357$, $T_g=131.5\text{K}$; 2. $\Delta P=0.30103$, $p=0.45\text{GPa}$, $T_m=210\text{K}$, $\theta_g=-0.3015$, $T_g=146.6\text{K}$; 3. $\Delta P=0.25589$, $p=0.38\text{GPa}$, $T_m=228\text{K}$, $\theta_g=-0.34009$, $T_g=150.5\text{K}$; 4. $\Delta P=0.21549$, $p=0.32\text{GPa}$, $T_m=240\text{K}$, $\theta_g=-0.37$, $T_g=150.5\text{K}$; 5- $\Delta\varepsilon=0$, $P_1-P_2=0$ (no volume change). The jumps of $\Delta\varepsilon_g$ at θ_g are equal to ΔP with $\Delta\varepsilon=0$.

3. The water phase diagram and the critical points under pressure

There is no first order transition at a critical point. Applying (2) and (3) with $\Delta\varepsilon=0$, and $P_1-P_2=0$, Line 1 and Line 2 in Figure 4 are shifted by $P=P_1=P_2$ under pressure at a critical point. In Figure 8, the LLPT line $\theta_{LL}=-0.16715$ ($T_{LL}=0.83235\times T_m$) extends from $P=-0.5$ to $P=0.8505$. A reduced temperature is used because it may apply to any melting temperature of any ice phase.

The critical points are determined assuming that Phase 3 resulting from a transformation of Phase 1 into Phase 2 at T_g continues to exist as a liquid phase when heated above the glass transition. Phase 3 in all glasses would have a superheating temperature above T_m called T_{n+} [1,eq(14)]*. There is no more LLPT above $P=0.8505$ because the homogeneous nucleation temperatures of strong Phase 1 and Phase 2 calculated with (5) and (7) reappear above θ_{LL} as shown in Figure 8.

Another critical point occurs for $P_1=0.006$ because the sum of latent heats of Phase 1 and Phase 3 at θ_{LL} is equal to zero as seen in Figure 4. These two critical points occur for $p_2/\rho_2=283.5$ and $p_1/\rho_1=2$ where ρ is the density in Kg.m^{-3} and p the pressure in Pascal. The pressure p_1 is equal to 18.3MPa with $\rho_1=915$ and $p_2=0.31\text{GPa}$ with $\rho_2=1093$ in rough agreement with other calculations [22,25,27,28] and with density measurements under pressure [59-61]. The new Phase 3 exists above T_g and explains the presence of a critical point at a low pressure equal to about 18.3MPa . This critical pressure slightly depends on the initial choice of T_g . It is equal to about $p=0$ for $T_g=135\text{K}$ instead of 136.6K .

The equations (2,3,10) applied at zero pressure indicate in Figure 4 that the first-order transformation during heating would be endothermic between $P=0.006$ and $P=0.8505$ and exothermic for $-0.5<P<0.006$ adding Phase 1 and Phase 3 contributions to the latent heat. The specific heat increase at zero pressure below T_m proves that the LLPT is always present for $P<0.006$ and exist at negative pressures down to $P=-0.5$. Phase 3 disappears with the glass transition for $P=-0.5$ when line 1 and line 2 in Figure 4 are shifted by -0.5 . This third critical point confirms that the stability limit of the two metastable water phases occurs for $p=-175\text{MPa}$ assuming a density $\rho=950\text{Kg.m}^{-3}$ [59]. This last critical point also corresponds in Figure 4 to the highest exothermic enthalpy under pressure and then, to the maximum density at negative pressure [62,63].

* The existence of a melting temperature above T_m due to superheating suggests that liquid Phase 3 could be ordered above T_g and T_m . An ordered liquid state has been already observed above T_g and above T_m in $\text{Zr}_{41.2}\text{Ti}_{13.8}\text{Cu}_{12.5}\text{Ni}_{10}\text{Be}_{22.5}$. [S. Wei, F. Yang, J. Bernarcik, I. Kaban, O. Shuleshova, A. Meyer, & R. busch, Nature Commun. 4 (2013) 2083].

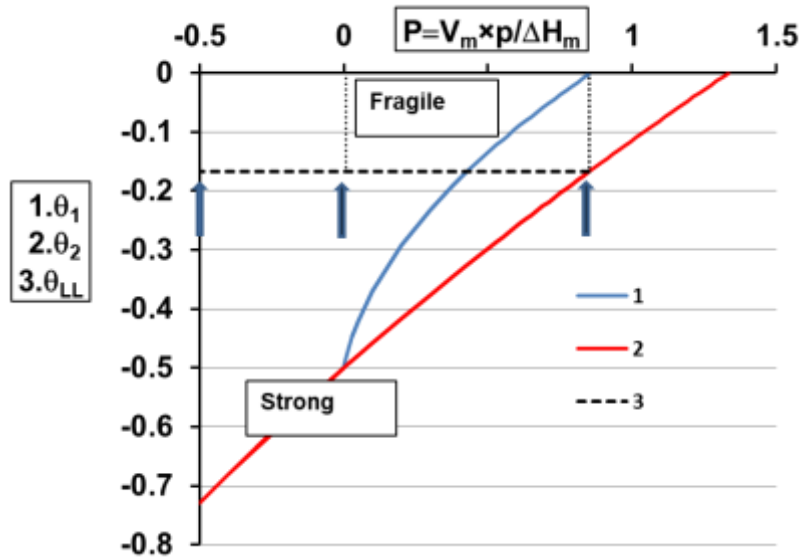


Figure 8 : Phase diagram of supercooled water at pressure p . Curves numbered from 1 to 3: 1- Homogeneous nucleation temperature of strong Phase 1 versus the enthalpy coefficient P induced by the pressure p ; 2- Homogeneous nucleation temperature of strong Phase 2 versus the enthalpy coefficient P induced by the pressure p ; 3- LLPT line separating the fragile liquid phase from the strong one at $\theta_{LL} = -0.16715$; first critical point: $P = -0.5$, $p \approx 175 \text{ MPa}$; second critical point: $P = 0.006$, $p \approx 18.3 \text{ MPa}$; third critical point, $P = 0.8505$, $p \approx 0.31 \text{ GPa}$.

Conclusion:

The thermodynamic parameters of two water phases, Phase 1 and Phase 2, separated by an enthalpy difference depending on $\theta^2 = (T - T_m)^2 / T_m^2$, have been determined only knowing the formation temperature of a strong glass in Phase 3 at $T_g = 136.6 \text{ K}$, the first-order LLPT at -45.6°C , the compressibility minimum at $+45.6^\circ \text{C}$, the ice melting heat $\Delta H_m = 6000 \text{ J/mole}$, and its melting temperature at 273.1 K .

The LDA phase of strong glass contains an enthalpy excess that increases its density to a value close to that of ice. The sharp transition temperatures T_{sg} observed after decompression, and the associated latent heats, are calculated in good agreement with experimental results. The enthalpy excess presence in this bulk glass leads, at a transformation temperature T_{sg} , to a thermodynamic equilibrium of amorphous ice instead of that of ultrastable glass.

Supercooled water is a fragile liquid above a liquid-to-liquid transition (LLPT) at $T_{LL} = 0.833 \times T_m$ that is transformed into a strong liquid below T_{LL} . The first-order character of LLPT disappears for three pressures equal to about -175 MPa , 18.3 MPa , and 0.31 GPa . Their presence shows that glass Phase 3 disappears for $p = -175 \text{ MPa}$ and becomes a liquid phase above T_g in the strong melt at higher pressures. The first-order LLPT line is exothermic by heating from -175 MPa to 18.3 MPa and endothermic from 18.3 MPa to 0.31 GPa .

Double glass transitions are predicted under pressure. The first-order glass-to-glass transitions under pressure, leading to high density amorphous phases called HDA and VHDA, result from the formation at temperatures T_{sg} of ultrastable polyamorphous states of Phase 3 under pressure. The enthalpy and volume reductions under pressure at these temperatures T_{sg} are constant and correspond to the enthalpy fraction frozen below $T_g=136.6\text{K}$ at zero pressure whereas the new glass transition temperature T_g and the melting temperature T_m vary under pressure.

REFERENCES

1. R.F. Tournier. *Chem. Phys. Lett.* **665** (2016) 64.
2. K.L. Kearns, K.R. Whitaker, M.D. Ediger, H. Huth, and C. Schick, *J. Chem. Phys.* 2010, **133** (2010), 014702.
3. S. Singh, M.D. Ediger, and J.J. de Pablo. *Nature Materials.* **12** (2013), 139.
4. K. Ishii, and H. Nakayama, *Phys. Chem. Chem. Phys.* **16** (2014), 12073.
5. R.F. Tournier, *Chem. Phys. Lett.* **641** (2015), 9.
6. O. Mishima, *Proc. Jap. Acad. Sci. B, Phys. Biol. Sci.* **86** (2010), 165.
7. T. Loerting, and N. Giovambattista,. Amorphous ice. *J. Phys.: Condens. Matter*, **18** (2006), R919.
8. O. Mishima. *Nature.* **384** (1996), 546.
9. O. Mishima, *J. Chem. Phys.* **100** (1994), 5910.
10. O. Mishima, L.D. Calvert & E. Whalley, *Nature*, **314** (1985), 76.
11. O. Mishima, L.D. Calvert, & E. Whalley. *Nature.* **340** (1984), 393.
12. T. Loerting, V.V. Brazhkin, T. Morishita. *Adv.Chem. Phys.* **143** (2009), 29.
13. W. Kauzmann, *Chem. Rev.* **43** (1948), 219.
14. C.A. Angell, M. Oguni, and W.J. Sichina, *J. Phys. Chem.* **86** (1982), 998.
15. C.A. Angell, *Chem. Rev.* 2002, **102** (2002), 2627.
16. J.A. McMillan and S.C.Los. *Nature.* **206** (1965), 806.
17. M. Sugisaki, H. Suga, and S. Seki. *Bull. Chem. Soc. Jap.* **41** (1968), 2586.
18. K. Amann-Winkel, C. Gainaru, P.H. Handle, M. Seidt, H. Nelson, R. Böhmer, and T. Loerting, *PNAS.* **110** (2013), 17720.
19. M. Oguni, S. Maruyama, K. Wakabayashi, and A. Nagoe, *Chem. Asian J.* **2** (2007), 514.
20. S. Maruyama, K. Wakabayashi, and M. Oguni. *AIP Conf. Proc.* **706** (2004), 675.

21. D. Liu, Y. Zhang, C.-C. Chen, C.-Y. Mou, P.H. Poole, and S.-H. Chen. *PNAS*. **104** (2007), 9570.
22. P.H. Poole, F. Sciortino, U. Essmann & H.E. Stanley. *Nature*. **360** (1992), 324.
23. V. Holten, C.E. Bertrand, M.A. Anisimov, and J.V. Sengers, *J. Phys. Chem.* **136** (2012), 094507.
24. C.A. Angell, J. Shuppert, and J.C. Tucker, *J. Phys. Chem.* **77** (1971) 3092.
25. S.V. Buldyrev, M. Canpolat, S. Havlin, O. Mishima, M.R. Sadr-Lahijany, A. Scala, F.W. Starr and H. Stanley, *AIP Conf. Proc.* **469** (1999), 243.
26. K. Ito, C.T. Moynihan & C.A. Angell, *Nature*. 398 (1999), 492.
27. V. Holten & M.A. Anisimov, *Sci. Rep.* 2 (2012) ,713.
28. J.C. Palmer, F. Martelli, Y. Liu, R. Car, A.Z. Panagiotopoulos, P.G. Benedetti, *Nature*. **510** (2014), 385.
29. P.F. McMillan, *Roy. Soc. Chem.* **14** (2004), 1506.
- 30- J. Souletie, *J. Phys. France*, **51** (1990) 883.
- 31- M.I. Ojovan, *J. Exp. Theor. Phys. Lett.* **79** (2004) 632.
- 32- M.I. Ojovan, *J. Exp. Theor. Phys.* **103** (2006) 819.
- 33- M.I. Ojovan, *J. Non-Cryst. Sol.* **382** (2013) 79.
- 34- M.I. Ojovan , W. E. Lee, *J. Non-Cryst. Sol.* **356** (2010) 2534.
- 35- D.S. Sanditov, M.I. Ojovan, *Physica B*, **523** (2017) 96.
- 36 R.P. Wool, *J. Polym. Sci. Pol. Phys.* **46** (2008)2765.
- 37- J.F. Stanzione III, K.E. Strawhecker, R.P. Wool, *J. Non-Cryst. Sol.* **357** (2011) 311.
- 38- S. Albert, Th. Bauer, M. Michl, G. Biroli, J.-P. Bouchaud, A. Loidl, P. Luckenheimer, R. Tourbot, C. Wiertel-Gasquet, F. Ladieu, *Science*, **352** (2016) 1308.
- 39- D. Ma, A.D. Stoica, X.-L. Wang, *Nature Mater.* **8** (2016) 30.
40. R.F. Tournier, *Physica B.* **454** (2014), 253.
41. R.F. Tournier *Phys. B. Condens. Matter.* **392** (2007), 79.
42. R.F. Tournier, J. Bossy. *Chem. Phys. Lett.* **658** (2016), 282.
43. R.F. Tournier, *Chem. Phys. Lett.* **651** (2016) 198; Corrigendum, **675** (2017), 174.
44. D.Turnbull, *J. Chem. Phys.* **20** (1952), 411.
45. K. Lu, Y. Li. *Phys. Rev. Lett.* **80** (1998), 4474.

46. K. Winkel, E. Mayer, and T. Loerting. *J. Phys. Chem.* **115** (2011), 14141.
47. J.J Shephard and C.G Salzmann.. *J. Phys. Chem. Lett.* **7** (2016), 2281.
48. R.F. Tournier *Materials.* **4** (2011), 869.
49. R.F. Tournier, *Sci. Technol. Adv. Mater.* **10** (2009), 014501.
50. R.F. Tournier. *Rev. de Metall.* **109** (2012), 27.
51. R.J. Speedy and C.A. Angell. *J. Chem. Phys.* **65** (1976), 851.
52. R.A. Millero, F.J. Fine *J.Chem. Phys.* **59** (1973), 5529.
53. C.A. Angell, W.J. Sichina, M. Oguni. *J. Phys. Chem.* **86** (1982), 998.
54. D. Bertolini, M. Cassettari, and G. Salvetti. *Chem. Phys. Lett.* **199** (1985), 553.
55. E. Tombari, C. Ferrari, G. Salvelli, *Chem. Phys. Lett.* **300** (1999), 749.
56. I.K. Ishii, H. Nakayama, S. Hirabayashi, M. Nakayama,. *Chem. Phys. Lett.* **459** (2008), 109.
- 57- L-M. Wang, S. Borick, C.A. Angell, *J. Non-Cryst. Sol.* **353** (2007), 3829.
- 58- L. Hornboll, Y. Yue, *J. Non-Cryst. Sol.* **354** (2008) 1862.
- 59- D.E. Hare, C.M. Sorensen, *J. chem. Phys.* **87** (1987) 4840.
- 60- T. Sorani, J. Arabas, H. Kubota,M. Kijima, *High Temp. High Pressures*, **32** (2000)433.
- 61- O. Mishima, *J. Chem. Phys.* **133** (2010) 144503.
- 62- C.A. Angell, *Nature Mat.* **13** (2014) 673.
- 63- M.E.M. Azouzi, C. Ramboz, J.-F. Lenain, and F. Caupin, *Nature Phys.* **9** (2013) 38.